PHYSICAL REVIEW B VOLUME 27, NUMBER 6 15 MARCH 1983

Ranges of low-energy, light ions in amorphous silicon

W. Wach* and K. Wittmaack
Physikalisch-Technische Abteilung, Gesellschaft für Strahlen- und Umweltforschung mbH, D-8042 Neuherberg, Federal Republic of Germany
(Received 8 September 1982)

Range profiles of (1–20)-keV Li, B, N, O, F, Na, Mg, and Al in amorphous Si have been measured by low-energy (≤ 3 keV) secondary-ion mass spectrometry. Mean projected ranges and standard deviations of these ranges were calculated from the as-measured profiles. In order to correct for bombardment-induced profile distortions, effective broadening parameters were extracted from the experimental data. The broadening parameters turned out to be element specific, varying between about 1 nm or less for Li, B, Na, and Al and up to ~ 12 nm for Mg. Corrected mean ranges and standard deviations are compared with tabulated data based upon Lindhard-Scharff-Schiøtt theory. At 10 keV, i.e., the lowest energy covered by tabulations, the experimental and theoretical ranges show very good agreement except for Na and Mg, in which case the measured ranges are 15–20% smaller than predicted. This discrepancy between experiment and theory is attributed to deviations of the projectile-target interaction potential from the assumed universal Thomas-Fermi potential. Range tabulations involving an empirical electronic stopping power, derived by a rigorous scaling and extrapolation of channeling measurements, are shown to be strongly in error in many cases.

I. INTRODUCTION

Ranges of low-energy ions in solids have been investigated in great detail recently. Work in this field has been motivated by the idea that range data can be used to derive the interaction potential between the swift ion and the target atom.[1,2] Most of the previous experimental range studies have been devoted to heavy ions implanted in light element targets, such as carbon, aluminum, and silicon, in which case the Rutherford backscattering technique can be employed for profile analysis.[3–10] The accuracy of this method is largely determined by the uncertainty in the stopping power of the probing beam. For helium in carbon, silicon, and germanium, experimental stopping-power data agree to within 5–15 % at energies between 300 keV and 2 MeV.[11]

While a large amount of low-energy range data is available for heavy ions, very few measurements have been reported for light ions. Since helium backscattering cannot be used for reason of interference of the signals due to substrate and dopant atoms, other methods have to be employed. Nuclear techniques[12–14] and secondary-ion mass spectrometry[15–17] (SIMS) are used most frequently. The SIMS technique has the advantage of being applicable to all elements. Moreover, isotope effects can be investigated under identical conditions.[17] Provided the energy of the probing beam is low ($\lesssim 3$ keV), deviations of the measured profile from the original concentration distribution may be negligible, at least for certain dopant-substrate combinations.[15,17] In this study we report on a systematic SIMS study of the range distribution of (1–20)-keV ^{6}Li, ^{7}Li, ^{10}B, ^{11}B, ^{14}N, ^{16}O, ^{19}F, ^{23}Na, ^{24}Mg, and ^{27}Al in amorphous silicon.

II. EXPERIMENTAL

Silicon samples, 10×10 mm^2, were cut from polished 2-in. wafers (thickness ~ 350 μm, orientation (100), resistivity 1 Ω cm, n-type). The native oxide on the samples was removed by etching in buffered HF. In order to produce an amorphous layer[18] the samples were first bombarded with 1×10^{15} argon ions/cm^2, using normally incident, raster-scanned beams of 50 keV Ar^+ or 100 keV Ar^{2+}. The corresponding depth to which the sample was rendered amorphous is estimated to be 40 and 80 nm, respectively.[19,20]

The dopant ions were produced as follows: Li^+ and Na^+ by a surface ionization source[21]; B^+, N^+, N_2^+, O^+, O_2^+, and F^+ by a plasma-type source[22,23] (using BCl_3, N_2, O_2, and SF_6, respectively, as supply gases; cold cathode operation in the case of O_2); Mg^+ and Al^+ by a sputter-ion

 ©1983 The American Physical Society

source.[24,25] Becoming amorphous and implanting were usually carried out using a 50-kV accelerator (base pressure in the sample chamber 3×10^{-6}Pa). Nitrogen and oxygen were implanted *in situ* in the SIMS instrument, thus avoiding surface contamination during sample transport in air.

The ion microprobe employed for depth profiling has been described elsewhere.[26,27] The instrument embodies the essential features of a high-performance device, such as raster-scanning bombardment in combination with electronic gating[28] as well as neutral-beam suppression.[29] Concentration profiles can be measured with a dynamic range[29] of up to 10^6. During analysis the pressure in the sample chamber was 3×10^{-7} Pa or less. Either Ar^+ or $O_2{}^+$ ions were used for sputtering and, in the latter case, also for secondary-ion yield enhancement.[30] Depth calibration was achieved by measuring the depth of the sputtered craters after profile analysis. A surface profilometer (Talysurf 10, Rank Taylor Hobson) was employed for this purpose.

The intensity of the sputtered Li^+, B^+, Si_2N^+, Si_2O^+, F^-, Na^+, Mg^+, and Al^+ ions was taken as a measure of the concentration of the respective dopant. The choice of $Si_2^+N^+$ and Si_2O^+ ions is based upon the finding that these species are emitted with rather high intensity (the intensities of N^+ and O^+ are low; N^- does not exist in stable form).

The implantation fluences were chosen so that the dynamic range in the subsequent profile analysis was better than 3×10^2. Depending upon the degree of ionization of the sputtered species[30,31] and the background due to adsorbed (and incorporated) gases,[32,33] the implantation fluences ranged from 5×10^{11} to 5×10^{15} ions/cm^2. Direct proportionality between the SIMS intensity and the dopant concentration was verified by depth profiling samples implanted with various fluences.

If the implantation fluence Φ and the depth Δx eroded per integration cycle are known, conversion of the (background-corrected) SIMS intensity I_j to the atomic fraction $c_i(x)$ of dopant (impurity) atoms is simple,

$$c_i(x)\simeq\langle c_i\rangle_j=(\Phi/n\,\Delta x)I_j\Big/\sum_{j=1}^{k}I_j, \tag{1}$$

where I_j is the intensity recorded in the depth interval $(j-1)\Delta x\cdots j\,\Delta x$. $\sum I_j$ is the total intensity accumulated in passing through the whole profile, i.e., $k\,\Delta x\geq x_m$, where x_m is the maximum range of the implanted ion (or the maximum depth at which a statistically relevant signal is detectable). $\langle c\rangle_j$ is an average concentration at the nominal depth $x=(j-0.5)\Delta x$. The deviation of $\langle c\rangle_j$ from the true concentration $c(x)$ depends upon the shape of the dopant concentration profile and the width δ of the electronic gate.[28] $\langle c\rangle_j\rightarrow c(x)$ for $\delta\rightarrow0$, provided one uses 1 frame per counting cycle.

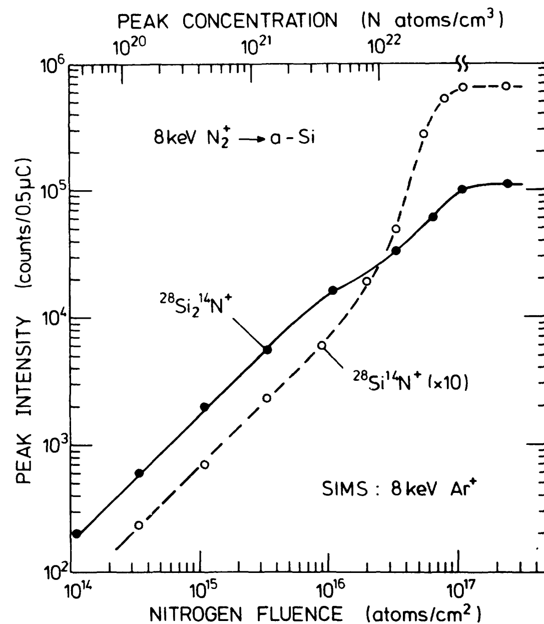

FIG. 1. Peak intensities of Si_2N^+ and SiN^+, recorded in SIMS analysis of 8-keV N_2 implantation profiles, vs the nitrogen fluence (bottom scale). The top scale represents the peak concentration calculated according to Eq. (1).

As an example, Fig. 1 shows the intensity of Si_2N^+ and SiN^+, measured at the peak of the 8-keV $N_2{}^+$ profiles, versus the implantation fluence. In the case of Si_2N^+ a linear relationship is observed up to nitrogen concentrations of about 2×10^{21} atoms/cm^3. Similar results were obtained for SiO^+ and Si_2O^+.[34]

In order to get an idea as to the effect of the energy deposition during sputtering on the shape of the profiles, some measurements were carried out with the probe energy as a parameter. Figure 2 shows depth profiles of 5 and 10 keV ^{6}Li and ^{7}Li recorded under impact of 2.5, 5, and 10 keV Ar. Marked changes in the profiles are seen only near the surface and in the long-range tails. As one would expect, the broadening effects become more evident the "narrower" the original dopant distribution. Note the interesting finding that ^{6}Li and ^{7}Li experience the same amount of relocation due to energy deposition by the probing beam (cf. the long-range tails of the 5-keV profiles in Fig. 2).

The results of Fig. 2 suggest that the profile distortions are quite small for depth profiling of Li in Si performed under 2.5-keV Ar impact. Similar conclusions were reached by the present authors for

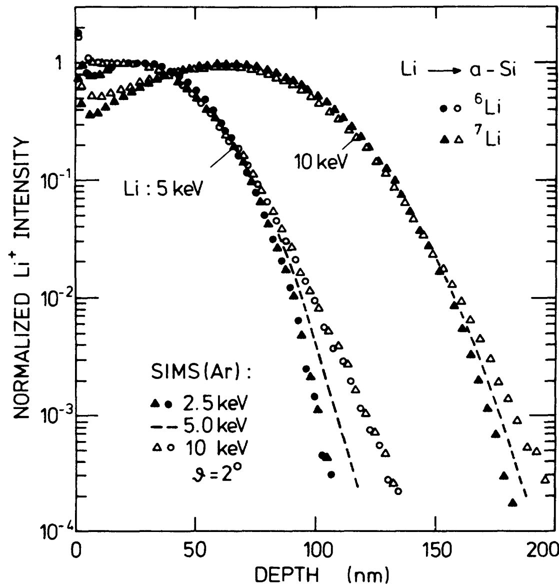

FIG. 2. Normalized depth profiles of 5 keV ^{6}Li and ^{7}Li and 10 keV ^{7}Li in amorphized silicon (*a*-Si). Parameter is the energy of the Ar^+ ions employed for sputter erosion in SIMS analysis.

the analysis of B in Si under low-energy O_2^+ impact.[16] The profiles reported below were measured under O_2^+ or Ar^+ bombardment at energies of 3 keV or less, as indicated in the respective figures.

III. RESULTS AND DISCUSSION

A. Range profiles

Normalized depth profiles of ^{6}Li, ^{7}Li, ^{14}N, ^{19}F, ^{23}Na, ^{24}Mg, and ^{27}Al in amorphous silicon (*a*-Si) are presented in Fig. 3. The profiles of ^{10}B and ^{11}B as well as of ^{16}O are omitted from Fig. 3; the boron profiles have been discussed in detail elsewhere,[17] the oxygen profiles were found to be almost identical to those of nitrogen (at the same implantation energy). In all cases an experimentally determined background intensity was subtracted from the measured profiles. The height of this background, relative to the peak intensity, varied between 5×10^{-5} (in the case of Li^+) to 3×10^{-3} (in the case of Si_2O^+).

B. Evaluation of range parameters

The experimental data were fed into a computer in order to calculate the mean projected ranges $\langle x \rangle$ and standard deviations $\langle(\Delta x)^2\rangle^{1/2}$. Low-energy results for boron in silicon are depicted in Fig. 4. As one would expect, the range parameters become very small as the implantation energy approaches zero. In fact, the data are not in disagreement with the natural assumption that $\langle x \rangle \rightarrow 0$ and $\langle(\Delta x)^2\rangle^{1/2} \rightarrow 0$ for $E \rightarrow 0$.

A rather different behavior is observed for nitrogen, as illustrated in Fig. 5. In this case a rigorous extrapolation to the limit of vanishing implantation energy results in rather large apparent range parameters, $\langle x \rangle|_{E\rightarrow 0} \equiv \delta_r \simeq 4.5$ nm and $\langle(\Delta x)^2\rangle^{1/2}|_{E\rightarrow 0} \equiv \delta_s \simeq 6$ nm. Similar effects are found for oxygen ($\delta_r \simeq 4$ nm, $\delta_s \simeq 6$ nm), fluorine ($\delta_r \simeq 2$ nm, $\delta_s \simeq 2.5$ nm), and magnesium ($\delta_r \simeq 11$ nm, $\delta_s \simeq 12.5$ nm) whereas lithium, sodium, and aluminum behave similar to boron, i.e., $\delta_r, \delta_s \lesssim 1$ nm.

The element-specific character of δ_r and δ_s is illustrated in Fig. 6. Also shown is the variation of the parameter λ which describes the inverse slope of the exponential tails in Fig. 3.[35] The cause and importance of δ_r, δ_s, and λ are discussed in the Appendix where it is shown that these parameters can be used to correct the as-measured range data for beam-induced broadening effects (atomic mixing and selective sputtering).

Corrected mean projected ranges and standard deviations for 10-keV light ions implanted in amorphous silicon are presented in Fig. 7. $\langle x \rangle$ and $\langle(\Delta x)^2\rangle^{1/2}$ decrease monotonically with increasing atomic number Z_1, for $3 \le Z_1 \le 9$. In the case of Na ($Z_1 = 11$) and Mg ($Z_1 = 12$) the projected ranges are somewhat lower than expected on the basis of the trend seen at lower atomic numbers. This nonmonotonic behavior is also noticeable in the Z_1 dependence of the standard deviations. However, the effect is less pronounced than in the case of the mean projected ranges.

The energy dependence of the mean projected ranges is depicted in Fig. 8. The data are plotted in Lindhard-Scharff-Schiøtt (LSS) units ξ and ϵ, where ξ is the reduced projected range (see below). The mean ranges derived in this study increase almost linearly with increasing energy, i.e., $\langle \xi \rangle \propto \epsilon^n$, with an exponent n between 0.95 and 1.1. Extrapolation of the present results to higher energies shows good agreement with data reported by other workers.[36–39]

C. Comparison with theory

According to Lindhard and co-workers[40–42] the slowing down of a swift ion in matter is due to elastic (nuclear) and inelastic (electronic) processes which are treated independently. In the *low-energy* region, which is characterized by the dominance of nuclear stopping, the ion energy E and the total range R are conveniently expressed in dimensionless reduced units ϵ and ρ (LSS units),[40]

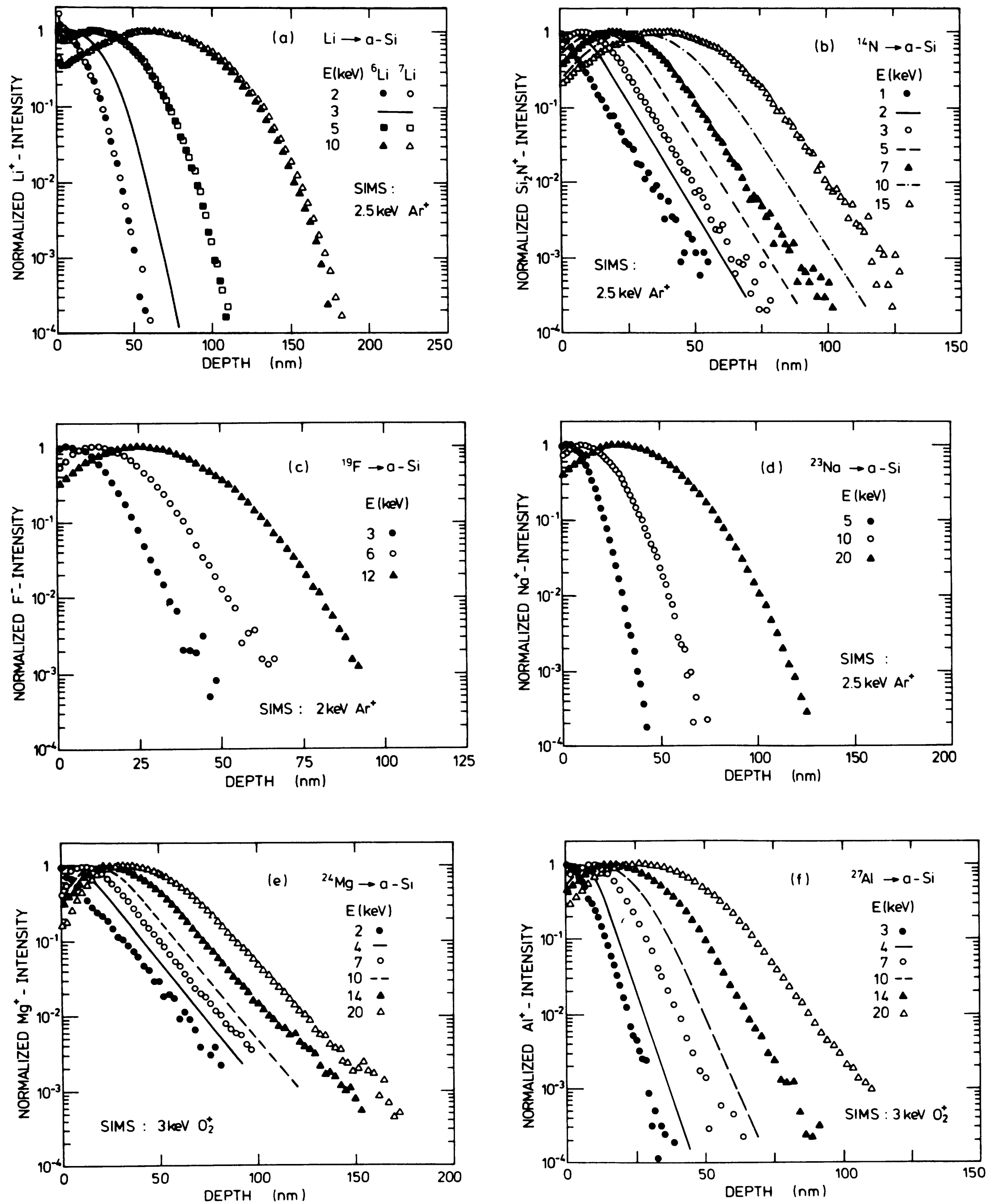

FIG. 3. Normalized SIMS depth profiles of implantation distribution of (a) ^{6}Li and ^{7}Li, (b) ^{14}N, (c) ^{19}F, (d) ^{23}Na, (e) ^{24}Mg, and (f) ^{27}Al in amorphized silicon (*a*-Si). For the sake of clarity some data points have been omitted.

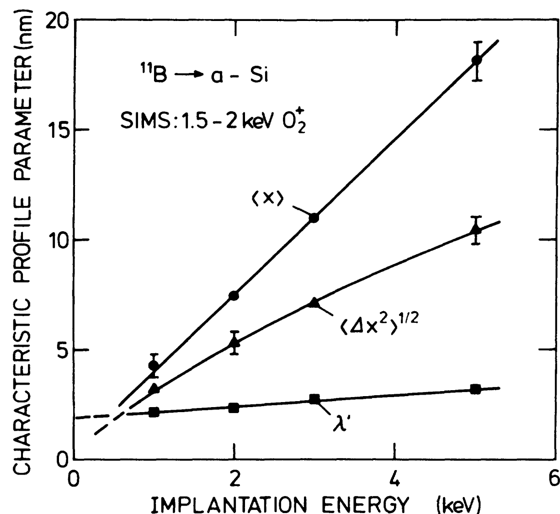

FIG. 4. Apparent mean range $\langle x \rangle$, standard deviation $\langle (\Delta x)^2 \rangle^{1/2}$, and apparent decay length λ' of ^{11}B implantation distributions in amorphized silicon vs the boron energy. SIMS analysis under impact of 1.5 keV O_2^+ at boron energies of 1 and 2 keV and 2 keV O_2^+ at 3 and 5 keV.

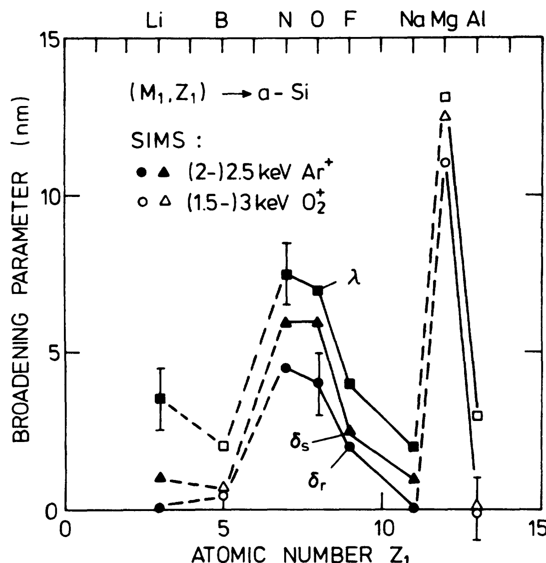

FIG. 6. Variation of the characteristic profile broadening parameters δ_r, δ_s, and λ vs the atomic number of the implanted ion.

$$\epsilon = a\mu E / Z_1 Z_2 e^2 (1+\mu) \tag{2}$$

and

$$\rho = \pi a^2 n \gamma R , \tag{3}$$

where a is the Thomas-Fermi screening radius, $a = 0.8853 a_0 (Z_1^{2/3} + Z_2^{2/3})^{-1/2}$, a_0 is the Bohr radius, e is the elementary charge, and n is the target density; Z_1, M_1, Z_2, and M_2 are the atomic numbers and mass numbers of the ion and the target atoms, respectively, $\mu = M_2/M_1$ and $\gamma = 4M_1M_2/(M_1+M_2)^2$.

If one assumes that the elastic interaction between the swift ion and target atoms can be described by a universal potential,[41] the reduced nuclear stopping power $(d\epsilon/d\rho)_n$ becomes a function of ϵ only. Thus, at sufficiently low energies, the reduced range ρ should also depend only on ϵ. This idea of similarity scaling of nuclear stopping was supported by the range measurements of Kalbitzer and

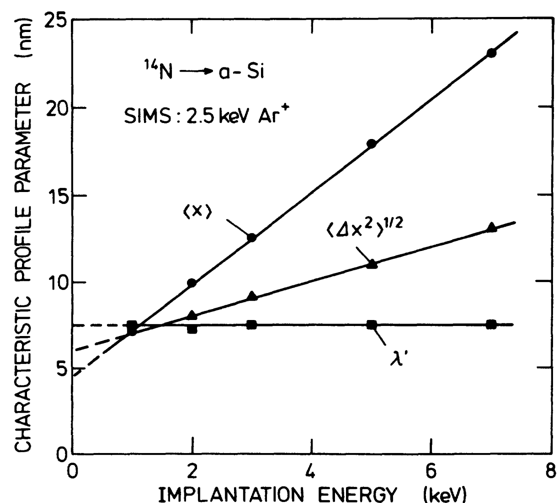

FIG. 5. Same as Fig. 4 except for ^{14}N implantation distributions in a-Si. Probing beam 2.5 keV Ar^+.

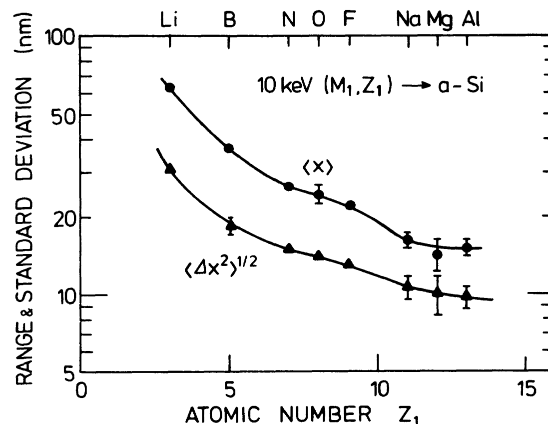

FIG. 7. Mean projected ranges and standard deviations in projected range for 10-keV light ions in amorphous silicon.

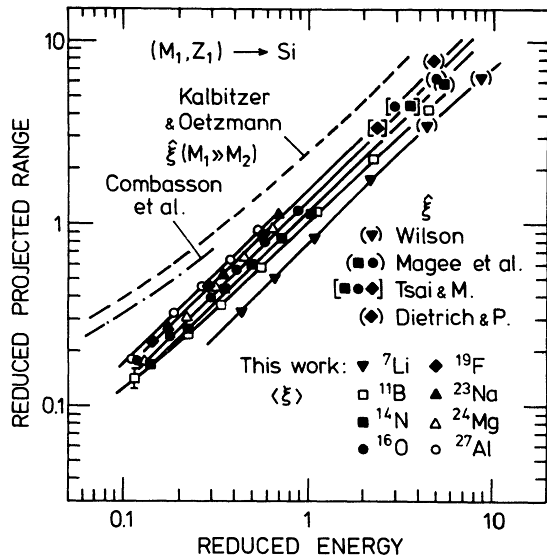

FIG. 8. Reduced mean projected ranges $\langle \xi \rangle$ for various elements in silicon vs the reduced energy ϵ. Most probable projected ranges $\hat{\xi}$ reported by other groups are shown for comparison: Combasson *et al.* (Ref. 8), Kalbitzer and Oetzmann (Ref. 9), Tsai and Morabito (Ref. 36), Dietrich and Plew (Ref. 37), Wilson (Ref. 38), and Magee *et al.* (Ref. 39). The element-specific symbols used for the data of this work have also been used for those of Refs. 36—39, but in parentheses.

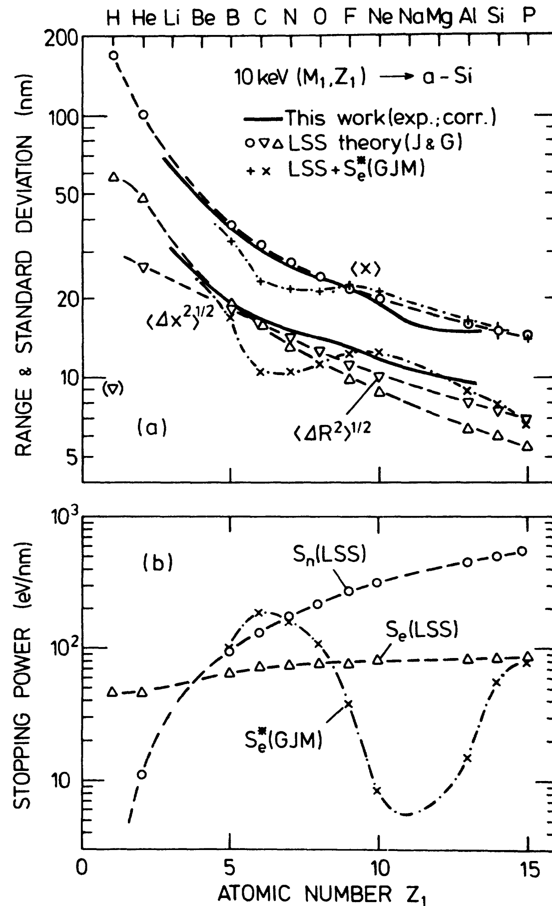

FIG. 9. (a) Comparison of the 10-keV range data of this study with calculations by Johnson and Gibbons (JG, Ref. 20) and Gibbons *et al.* (GJM, Ref. 44). $\langle (\Delta R)^2 \rangle^{1/2}$ is the standard deviation in the total range. (b) Nuclear and electronic stopping powers, S_n and S_e, of silicon for 10-keV projectiles of low atomic number. The stopping powers based upon LSS theory (Ref. 12) were taken from Ref. 24. The dashed-dotted curve shows the modified electronic stopping power S_e^* employed by Gibbons *et al.* in calculating the respective range data in (a).

Oetzmann[9] which, for heavy ions in light-element targets, suggest the validity of a universal interaction potential at reduced energies ϵ between 4×10^{-5} and 3. More detailed investigations by Besenbacher *et al.*,[10] however, revealed pronounced Z_1 oscillations of heavy-ion ranges in amorphous silicon at a fixed energy $\epsilon=1.5\times10^{-2}$. Maxima and minima were found for elements around noble metals and noble gases, respectively, with a peak-to-peak variation of up to 40%. Measurements of the energy dependence showed that deviations from the (ρ,ϵ) scaling increase with decreasing energy below $\epsilon=4\times10^{-2}$. Consequently, the assumption of a universal interaction potential is not justified at large interatomic separation. Similar conclusions were reached by Loftager *et al.*[43] on the basis of differential scattering cross-section measurements.

The present results may be compared with tabulated range data[20,44,45] calculated on the basis of LSS theory. A compilation of data for the lowest energy covered by the range tables, i.e., 10 keV, is shown in Fig. 9. The open symbols and crosses represent calculations by Johnson and Gibbons[20] (JG) and Gibbons, Johnson, and Mylroie[44] (GJM), respectively. It is evident that the mean projected ranges calculated by JG are in rather good agreement with the present results [solid line in Fig. 9(a)], except for the "dip" found experimentally in the Na-Mg region. In the case of the projected range straggling, on the other hand, the agreement between experiment and the calculations by JG is good only for atomic numbers $Z_1\le6$. For $Z_1\ge7$ the experimental results are better represented by the calculated standard deviation in the total range, $\langle(\Delta R)^2\rangle^{1/2}$. This kind of discrepancy between calculated and measured straggling was noted previously by other groups for the case of heavy ions implanted in silicon[46] or dielectric layers.[47] According to Smith[45] the error in the nu-

merical calculations appears to be in the expansion used for the LSS equations. Insufficient terms were used which effectively resulted in the elimination of all contributions to $\langle(\Delta x)^2\rangle^{1/2}$, which are due to the variation in energy loss on collisions. Consequently, the calculated value of $\langle(\Delta x)^2\rangle^{1/2}$ reflects only the straggling produced by angular variations on impact.

Improved numerical procedures have been employed by GJM in preparing a new set of range tabulations.[44] At the same time, however, GJM replaced the LSS electronic stopping power originally used[20] by an empirical formula which involved a rather doubtful scaling procedure. It was assumed that the ratio of the electronic stopping powers of crystalline and amorphous silicon, $S_e\langle 110\rangle/S_e$(amorphous), is a constant for a given projectile and energy. S_e(a-Si,Z_1) was thus derived from S_e($\langle 110\rangle$Si,Z_1) and S_e(a-Si, ^{11}B), measured by Eisen[48] and Eisen *et al.*,[49] respectively, at energies between about 100 and 500 keV. Extrapolation to lower and higher energies was achieved by assuming that the dependence $S_e\langle 110\rangle \propto E^p$ observed by Eisen[48] is valid at all energies of interest. Since the measured p values range from 0.29 (for ^{14}N) to 0.89 (for ^{24}Mg), deviations from the velocity-proportional ($p=0.5$) LSS electronic stopping power must become quite large at energies as low as 10 keV.

The effect is illustrated in Fig. 9(b). Whereas the scaled electronic stopping power S_e^*(GJM) for ^{12}C and ^{14}N in a-Si is a factor of 2–3 larger than S_e(LSS), the scaled value for ^{20}Ne amounts to only 10% of the LSS-theory prediction. Depending on the ratio S_e^*/S_n the oscillations in S_e^* are also evident in the calculated values for $\langle x\rangle$ and $\langle(\Delta x)^2\rangle^{1/2}$; cf. Fig. 9(a). Clearly, the present range data do not support the scaling procedure employed by GJM.[44] (S_e^* was also used in the range calculations of Smith.[45]) The incorrectness of the GJM scaling procedure was pointed out previously by Dietrich and Plew[37] on the basis of range measurements of 100 to 500 keV ^{19}Fe in Si.

Returning to Fig. 8, one will note that at a fixed energy ϵ, the (reduced) projected range ξ decreases with increasing mass of the incident ion. This is largely due to the fact that the projection factor $\langle x\rangle/\langle R\rangle=\langle\xi\rangle/\langle\rho\rangle$ decreases with increasing mass ratio M_2/M_1.[40,42] The effect is illustrated in Fig. 10 which shows a comparison of the theoretical low-energy projection factor (dashed line) with experimental projected ranges relating to a fixed energy $\epsilon=0.35$ (data derived from Fig. 8 by interpolation or extrapolation). The results of this work exhibit the same trend as the theoretical predictions except for the Na-Mg data which are about 10–15% smaller than expected on the basis of the ranges

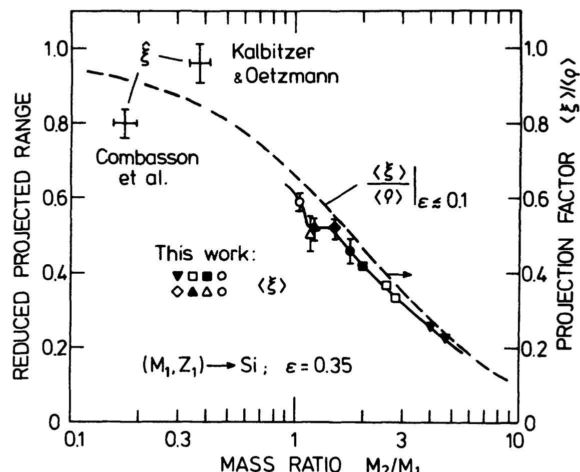

FIG. 10. Reduced projected ranges vs target-to-projectile mass ratio at a fixed reduced energy $\epsilon=0.35$. The data due to Combasson *et al.* (Ref. 8) and Kalbitzer and Oetzmann (Ref. 9) are shown for comparison. The dashed curve shows the theoretical projection factor $\langle\xi\rangle/\langle\rho\rangle=\langle x\rangle/\langle R\rangle$ for r^{-3} potentials and vanishingly small electronic stopping (Ref. 42).

measured at other mass ratios. Note the interesting finding that the projected ranges for different isotopes (^{6}Li, ^{7}Li, ^{10}B, and ^{11}B) fall on the same curve. The observation of identical low-energy projected ranges of ^{6}Li and ^{7}Li [cf. Fig. 3(a)] as well as of ^{10}B and ^{11}B (Ref. 17) in Si, at a fixed implantation energy, may thus be explained by stating that the larger nuclear stopping power for the heavier isotope is compensated (almost) completely by less pronounced angular scattering which in turn leads to a larger projection factor.

It should be mentioned that a reduced energy $\epsilon=0.35$ corresponds to an energy of 10 keV for ^{23}Na incident on Si. In that case the electronic contribution to the total stopping power amounts to about 20%; cf. Fig. 9(b). Since S_n decreases much more slowly than S_e at reduced energies below 0.35 [for Thomas-Fermi interaction the maximum of S_n is located at $\epsilon\simeq 0.3$ (Ref. 41)], the projected ranges shown in Fig. 10 are largely (to about 90%) due to nuclear stopping. Consequently, the dip in the Z_1 dependence of the ranges, noted in Figs. 7 and 10 for Na and Mg, must be attributed to the fact that the nuclear stopping power for the above elements is larger than expected on the basis of a monotonic Z_1 dependence of S_n. [If *small* oscillations in the random electronic stopping power were to exist with the same general form as in Fig. 9(b), this would make the deduced nonmonotonic variation of S_n even larger.]

To our knowledge, deviations from a monotonic

Z_1 dependence of low-energy ranges have previously not been reported for *light* projectiles ($Z_1 \leq 13$). For *heavy* ions ($18 \leq Z_1 \leq 92$) in silicon, however, Besenbacher *et al.*[10] reported Z_1 oscillations in projected range which become clearly evident at reduced energies below about 0.06. These oscillations have been attributed to deviations of the projectile-target interaction potential from a universal function.[10] The present results suggest that element-specific potentials are also required to describe nuclear stopping in silicon for projectiles of low atomic number. Quantitative information as to the form of the interaction potential is not available at present. In order to proceed in this direction it would be desirable to compare the results of this study with numerical range calculations.

IV. CONCLUSION

Using low-energy SIMS, we have shown that shallow range profiles in silicon can be measured with high accuracy. In many cases bombardment-induced effects can be kept sufficiently small so that projected ranges and standard deviations can be determined directly from the measured profiles. Excessive profile distortions, observed with N, O, and Mg in Si, can be taken into account on the basis of an analysis of the profile tails as well as of the energy dependence of the as-measured range parameters. The projected ranges derived experimentally are generally in good agreement with predictions of the LSS theory which involves the use of a (universal) Thomas-Fermi interaction potential. In the case of Na and Mg, the observed ranges are 10–15% smaller than expected from the trend found with the neighboring elements. This result is interpreted in terms of a nonmonotonic Z_1 dependence of the interaction potential between the swift ion and a target atom.

APPENDIX

In order to understand the nonzero values for δ_r and δ_s we return to Fig. 3. Within experimental accuracy, all profiles become exponential in the long-range tails, i.e.,

$$I/\widetilde{I}=\exp[-(x-\widetilde{x})/\lambda'], \tag{A1}$$

where $\widetilde{I}=I(x=\widetilde{x})$ is the intensity at the reference plane and λ' some characteristic decay length. Analysis of the experimental data shows that δ_r and δ_s become large whenever λ' is large; cf. Fig. 6. In such cases the tails become exponential already at rather high levels of the normalized intensity [e.g., in Figs. 3(b) and 3(e)].

Note that λ' varies comparatively little with increasing implantation energy E (cf. Figs. 4 and 5). The parameter $\lambda=\lambda'$ $(E\rightarrow 0)$ may thus be determined rather easily. λ has previously been interpreted in terms of atomic mixing and selective sputtering.[35,50] The idea is that energy deposition by the probing beam will cause collisional relocation of target atoms and in some cases also cause damage-enhanced diffusion. Owing to this beam-induced mixing effect the original dopant (impurity) distribution $c_i(x)$ will be altered as the surface recedes during sputtering. Additional changes in the near-surface concentration of dopants will result if the escape functions of dopant and host atoms are not identical (selective sputtering).

The measured SIMS intensity $I_i(x)$ may be written

$$I_i(x)=\eta_i\alpha_i A\dot{\phi}\int_0^\infty \gamma_i(x')\widetilde{c}_i(x+x')dx', \tag{A2}$$

where $\widetilde{c}_i$ is the altered impurity distribution, α_i is the degree of ionization, γ_i is the escape function of impurity atoms, η_i is an instrumental factor, A is the "gated" area, $\dot{\phi}$ is the flux density of the probing beam, and x' is the distance from the instantaneous surface. Equation (A2) implies that γ_i is independent of $\widetilde{c}_i$, an assumption which should be valid for the concentration levels of interest in this work. Moreover, α_i is assumed to be independent of the depth of origin of sputtered atoms.

An accurate determination of $c_i(x)$ by deconvolution of $I_i(x)$ does not seem possible at present because neither $\gamma_i(x)$ nor the details of the mixing process are known well enough. In view of the fact that the broadening parameters observed in this work vary nonmonotonically with the atomic number of the dopant, collisional relocation[51,52] does not seem to be the only source of mixing.

We have recently pointed out[35,50] that information about the combined effect of mixing and selective sputtering can be deduced from the slope of the exponential tails. If during sputtering implanted atoms are still released, although the bombarded surface has already receded beyond the maximum depth of doping, these atoms must have lost memory of the site where they originally came to rest after implantation. The distribution of dopant atoms retained in the sample may then be described by a normalized "mixing profile" $p_i(x)$, which maintains a constant *shape* as sputtering proceeds.[50] Thus

$$I_i(x)=\eta_i\alpha_i A\dot{\phi} n^{-1}N_i(x)\int_0^\infty \gamma_i(x')p_i(x')dx, \tag{A3}$$

where $N_i(x)$ is the areal density (atoms/cm^2) of impurities retained in the sample after sputtering to depth x and n is the density of the matrix

(atoms/cm^3). Normalization of $p_i(x)$ reads

$$\int_0^\infty p_i(x')dx'=1. \quad (A4)$$

The integral in Eq. (A3) can be shown to be related to λ in the form[35]

$$\lambda=Y_m \Big/ \int_0^\infty \gamma_i(x')p_i(x')dx, \quad (A5)$$

where Y_m is the sputtering yield of the host matrix. Thus

$$I_i(x)=\eta_i\alpha_i A(\dot{x}/\lambda)N_i(x), \quad (A6)$$

where $\dot{x}$ is the erosion rate of the sample $\dot{x}=Y_m\dot{\phi}/n$.

Note the similarity of Eqs. (A2) and (A3) which implies that the broadening parameters δ_r and δ_s are correlated with the decay length λ (cf. Figs. 4–6). In the present context the main purpose of determining λ is to allow a more accurate assessment of δ_r and δ_s in all those cases where the observed broadening effect was small.

It must be pointed out that although λ can be determined easily from sputter profiles, experiments of that kind do not provide any information about the escape function $\gamma_i(x)$ and the mixing profile $p_i(x)$. These functions can only be determined by experiments in which the depth distribution of mixed dopants is determined. (By contrast, λ reflects merely the fluence dependence of dopant removal from an intermixed sample.)

Phenomenologically, the measured profile $c'(x)$ may be considered as the result of a convolution of the original implantation distribution $c(x)$ and a broadening function $f(x)$, which is supposed to reflect the combined effect of mixing and selective sputtering. Then[53]

$$\langle x\rangle_{c'}=\langle x\rangle_c+\langle x\rangle_f \quad (A7)$$

and

$$\langle(\Delta x)^2\rangle_{c'}=\langle(\Delta x)^2\rangle_c+\langle(\Delta x)^2\rangle_f. \quad (A8)$$

The amount and direction by which $\langle x\rangle_c$ is shifted will thus depend on the symmetry and the peak position of $f(x)$. If we assume that the depth sputtered before arriving at a stationary state in mixing is small compared to $\langle x\rangle_c$ and $\langle(\Delta x)^2\rangle_c^{1/2}$, the correction terms can be derived directly from Figs. 4–6, i.e., we have $\langle x\rangle_f\equiv\delta_r$ and $\langle(\Delta x)^2\rangle_f^{1/2}=\delta_s$.

To obtain the actual $\langle x\rangle$ and $\langle(\Delta x)^2\rangle^{1/2}$ values, we have used Eqs. (A7) and (A8) and the data of Fig. 6 for nitrogen, oxygen, fluorine, and magnesium. In the case of lithium, boron, sodium, and aluminum, the as-measured data are considered to be affected only to a negligible extent since δ_r and δ_s amount to only 1 nm or less.

*Present address: Siemens AG, Data Processing Department, D-8000 München 83, Federal Republic of Germany.

[1]S. Kalbitzer and H. Oetzmann, Phys. Lett. 59A, 197 (1976).
[2]W. D. Wilson, L. G. Haggmark, and J. P. Biersack, Phys. Rev. B 15, 2458 (1977).
[3]J. S. Williams and W. A. Grant, Radiat. Eff. 25, 55 (1975).
[4]A. Feuerstein, S. Kalbitzer, and H. Oetzmann, Phys. Lett. 51A, 165 (1975).
[5]H. H. Andersen, J. Bøttiger, and H. Wolder Jørgensen, Appl. Phys. Lett. 26, 678 (1975).
[6]P. Blank and K. Wittmaack, Phys. Lett. 54A, 33 (1975).
[7]R. A. Baragiola, D. Chivers, D. Dodds, W. A. Grant, and J. S. Williams, Phys. Lett. 56A, 371 (1976).
[8]J. L. Combasson, B. W. Farmery, D. McCulloch, G. W. Neilson, and M. W. Thompson, Radiat. Eff. 36, 149 (1978).
[9]S. Kalbitzer and H. Oetzmann, Radiat. Eff. 47, 57 (1980).
[10]F. Besenbacher, J. Bøttiger, T. Laursen, P. Loftager, and W. Möller, Nucl. Instrum. Methods 170, 183 (1980).
[11]H. Oetzmann and S. Kalbitzer, Radiat. Eff. 47, 73 (1980).
[12]J. F. Ziegler *et al.*, Nucl. Instrum. Methods 149, 1 (1978).
[13]F.-J. Demond, S. Kalbitzer, H. Mannsperger, and G. Müller, Nucl. Instrum. Methods 168, 69 (1980).
[14]J. Biersack, D. Fink, R. Henkelmann, and K. Müller, Nucl. Instrum. Methods 149, 93 (1978).
[15]C. W. Magee, S. A. Cohen, D. E. Voss, and D. K. Brice, Nucl. Instrum. Methods 168, 383 (1980).
[16]K. Wittmaack and W. Wach, Nucl. Instrum. Methods 191, 327 (1981).
[17]W. Wach and K. Wittmaack, Nucl. Instrum. Methods 194, 113 (1982).
[18]J. R. Dennis and E. B. Hale, Appl. Phys. Lett. 29, 523 (1976).
[19]P. Sigmund, Rev. Roum. Phys. 17, 969 (1972).
[20]W. S. Johnson and J. E. Gibbons, *Projected Range Statistics in Semiconductors,* (Stanford University Press, Stanford, 1969).
[21]R. K. Feeney, W. E. Sayle, and J. W. Hooper, Rev. Sci. Instrum. 47, 964 (1976).
[22]C. E. Carlston and G. D. Magnuson, Rev. Sci. Instrum. 33, 905 (1962).
[23]K. Wittmaack, J. Vac. Sci. Technol. 16, 1027 (1979).
[24]K. J. Hill and R. S. Nelson, Nucl. Instrum. Methods 38, 15 (1965).
[25]W. Wach and K. Wittmaack (unpublished).

[26]K. Wittmaack, in *Ion Beam Surface Layer Analysis,* edited by O. Meyer, G. Linker, and F. Käppeler (Plenum, New York, 1976), Vol. 2, p. 649.

[27]K. Wittmaack, Vacuum 32, 65 (1982).

[28]K. Wittmaack, Appl. Phys. 12, 149 (1977).

[29]K. Wittmaack and J. B. Clegg, Appl. Phys. Lett. 37, 285 (1980).

[30]K. Wittmaack, Nucl. Instrum. Methods 168, 343 (1980).

[31]P. Williams, Surf. Sci. 90, 588 (1979).

[32]W. Wach and K. Wittmaack, in *Secondary Ion Mass Spectrometry SIMS II,* edited by A. Benninghoven, C. A. Evans, Jr., R. A. Powell, R. Shimizu, and H. A. Storms (Springer, Berlin, 1979), p. 85.

[33]W. Wach and K. Wittmaack, J. Appl. Phys. 52, 3341 (1981).

[34]K. Wittmaack, Surf. Sci. 112, 168 (1981).

[35]W. Wach and K. Wittmaack, Surf. Interf. Anal. 4, 230 (1982).

[36]I. C. C. Tsai and J. M. Morabito, in *Ion Implantation in Semiconductors,* edited by S. Namba (Plenum, New York, 1975), p. 115.

[37]H. B. Dietrich and L. E. Plew, Appl. Phys. Lett. 29, 406 (1976).

[38]R. G. Wilson, Radiat. Eff. 46, 141 (1980).

[39]C. W. Magee, J. C. Bean, G. Foti, and J. M. Poate, Thin Solid Films 81, 1 (1981).

[40]J. Lindhard, M. Scharff, and H. E. Schiøtt, Mat. Fys. Medd. Dan. Vid. Selsk. 33, No. 14 (1963).

[41]J. Lindhard, V. Nielsen and M. Scharff, Mat. Fys. Medd. Dan. Vid. Selsk. 36, No. 10 (1968).

[42]H. E. Schiøtt, Radiat. Eff. 6, 107 (1970).

[43]P. Loftager, F. Besenbacher, O. S. Jensen, and V. S. Sørensen, Phys. Rev. A 20, 1443 (1979).

[44]J. F. Gibbons, W. S. Johnson, and S. W. Mylroie, *Projected Range Statistics,* 2nd ed. (Dowden, Hutchinson and Ross, Stroudsburg, 1975).

[45]B. Smith, *Ion Implantation Range Data for Silicon and Germanium Device Technologies* (Learned Information, Oxford, 1977).

[46]B. L. Crowder, J. Electrochem. Soc. 118, 943 (1971).

[47]W. K. Chu, B. L. Crowder, J. W. Mayer, and J. F. Ziegler, Appl. Phys. Lett. 22, 490 (1973).

[48]F. H. Eisen, Can. J. Phys. 46, 561 (1968).

[49]F. H. Eisen, B. Welch, J. E. Westmoreland, and J. W. Mayer, in *Atomic Collisions in Solids,* edited by D. W. Palmer, M. W. Thompson, and P. D. Townsend (Pergamon, London, 1970), p. 111.

[50]K. Wittmaack, J. Appl. Phys. 53, 4817 (1982).

[51]P. Sigmund and A. Gras-Marti, Nucl. Instrum. Methods 168, 389 (1980).

[52]A. Gras-Marti and P. Sigmund, Nucl. Instrum. Methods 180, 211 (1981).

[53]R. N. Bracewell, *The Fourier Transform and its Applications,* 2nd ed. (McGraw-Hill, New York, 1978).